Dependence of the magnetization reversal of Fe/Tb multilayers on layer thickness and growth temperature

1999 J. Phys.: Condens. Matter 11 4317

(http://iopscience.iop.org/0953-8984/11/22/303)

J. Phys.: Condens. Matter **11** (1999) 4317–4328. Printed in the UK PII: S0953-8984(99)97242-9

Dependence of the magnetization reversal of Fe/Tb multilayers on layer thickness and growth temperature

W S Kim, W Kleemann, R A Brand and W Keune

Laboratorium für Angewandte Physik, Gerhard Mercator-Universität, D-47048 Duisburg, Germany

Received 4 September 1998, in final form 17 March 1999

Abstract. Fe/Tb multilayers (MLs) with Fe and Tb layer thicknesses $t_{Fe} = 1$–5 nm and $t_{Tb} = 1.9$ nm are prepared by thermal evaporation at substrate temperatures $T_s = 150$ (LT) and 300 K (HT), and investigated by means of the magneto-optical Kerr ellipticity, ε_K, at temperatures in the range $50 \leqslant T \leqslant 300$ K. Amorphous Fe, a-Fe, is encountered for $t_{Fe} < 3.0$ and 2.5 nm in LT and HT MLs, respectively, a small fraction of which is weakly exchange coupled at all temperatures. Perpendicular magnetic anisotropy (PMA) induced by the antiferromagnetically coupled Fe/Tb interfaces is observed on all MLs unless $t_{Fe} \geqslant 4$ nm, where in-plane anisotropy dominates. In LT MLs with thick a-Fe layers, $t_{Fe} = 3$ nm, a transition from Fe-dominated interface PMA to Tb-dominated bulk PMA with extreme coercivity, $H_c > 4$ MA m^{-1}, is observed below 200 K. Field-induced decoupling effects give rise to peculiar hysteresis cycles in the crossover range $160 < T < 210$ K. In HT MLs, sharp interfaces bear characteristics of the two-dimensional Ising model in the temperature range T_c(a-Fe) ≈ 200 K $< T < T_c$(Fe/Tb) ≈ 330 K.

1. Introduction

Compositionally modulated multilayers (MLs) of rare earths (RE) and transition metals (TM) have been intensively studied because of their potential application in magneto-optic recording [1] and because of their interesting physical properties, including magnetic coupling [2] and perpendicular magnetic anisotropy (PMA) [3]. For example, amorphous Fe/Tb (a-Fe/Tb) MLs show strong PMA even at room temperature (RT), independently of the techniques used to prepare them, e.g. sputtering [4] or evaporation [5]. A strong deviation in magnetic properties between MLs grown by different preparation techniques is found in crystalline Fe/Tb (α-Fe/Tb) MLs. PMA is never observed in sputtered MLs with Fe thicknesses of $t_{Fe} \geqslant 2.3$ nm [4] in contrast with evaporated MLs, where the PMA is observed up to $t_{Fe} = 3.5$ nm [5–7]. It is well known that preparation conditions strongly influence the magnetic properties and crystallographic structures [8]. In particular, the substrate temperature is crucial in the determination of the extents of the interfaces [9], their crystallographic structures [10] and their magnetic properties [11].

In this paper we reveal the effects of different substrate temperatures on the formation of amorphous Fe_XTb_{1-X} alloys located at the interfaces of Fe/Tb MLs and their morphological, magnetic and magneto-optic properties, by measuring the polar Kerr ellipticity (ε_K) as a function of temperature within the range $50 \leqslant T \leqslant 300$ K.

Special attention is paid to a novel soft-magnetic amorphous Fe (a-Fe) component. As observed for Fe/Tb/Ag MLs [12], it seems to be nearly uncoupled from the remainder of the ML system and does not change its properties with the change from crystalline to amorphous

0953-8984/99/224317+12$19.50

MLs. On the other hand, we investigate the temperature dependence of the total ferrimagnetic moment at the 'compensation transition' in addition to its dependence on the ML geometry. Whereas the temperature-controlled compensation point for amorphous FeTb alloys is rather sharply defined [13], the situation is more complex for Fe/Tb MLs, where only the interface is alloyed. A special situation is encountered if layers of a-Fe are intercalated; these order magnetically in the same temperature range as Tb, $T \approx 200$ K. Here, a peculiar competition between field and exchange energy is observed at high fields, $H \approx 5$ MA m^{-1}.

2. Experimental details

Fe/Tb multilayers (MLs) are prepared in ultrahigh vacuum by thermal evaporation onto Si(111) substrates at different substrate temperatures, $T_s = 150$ and 300 K. The pressure is kept below 1×10^{-9} mbar during evaporation. The deposition rate and film thickness are monitored by calibrated quartz microbalances located close to the substrate position. The deposition is held at a rate of 0.02 nm s^{-1} for Fe and Tb. The thickness of Fe, t_{Fe}, is varied from 1.0 to 5.0 nm at constant Tb thickness, $t_{Tb} = 1.9$ nm. The total thickness of the films corresponds to 19 Fe/Tb bilayers capped by an additional top layer of Fe with thickness t_{Fe}. The samples are investigated by means of the polar magneto-optic Kerr effect (MOKE) at a light wavelength $\lambda = 633$ nm and at temperatures $50 \leqslant T \leqslant 300$ K in applied magnetic fields $|H| \leqslant 4.8$ MA m^{-1} by applying a polarization modulation technique using a photoelastic modulator and a Babinet–Soleil compensator [14].

3. Results and discussion

3.1. Thickness dependence

Figure 1 shows the polar Kerr ellipticity (ε_K) curves of the Fe/Tb MLs with fixed Tb thickness, $t_{Tb} = 1.9$ nm, and various Fe thicknesses, $t_{Fe} = 1.5$, 3.0 and 5.0 nm. They were obtained at room temperature (RT) after preparation at '*low*' and '*high*' substrate temperatures, $T_s = 150$ K (LT, figure 1(a)) and 300 K (HT, figure 1(b)). A first glance at the hysteresis curves thus obtained immediately shows that they depend strongly not only on the thickness t_{Fe}, but also on T_s. The HT hysteresis loops (figure 1(b)) reveal complex structures, which strongly differ from the more uniform ones obtained for the LT MLs (figure 1(a)). As will be discussed below, this is connected with structural heterogeneity of the MLs involving different modifications of Fe and interface alloying of Fe with Tb [15].

There are also common properties observed for both LT and HT MLs. In both series the sign of the MOKE signal changes in the range $1.5 \leqslant t_{Fe} \leqslant 2.0$ nm. Since the MOKE signal is primarily due to the TM component [16] and ferrimagnetic coupling is encountered in the case of Fe/Tb [17], a change of sign in ε_K signifies a compensation point as observed for Fe/Tb MLs prepared by sputtering techniques [18]. Furthermore, a changeover from PMA to in-plane anisotropy is observed for LT and HT MLs in the interval $3.0 < t_{Fe} < 5.0$ nm. The magnetization loops change from rectangular and hysteretic to oblique and reversible with saturation fields $H_s \approx 1$ MA m^{-1}.

Some correlations between the magneto-optic and the magnetic properties of the LT MLs (figure 1(a)) are illustrated in figure 2, where the saturated MOKE ellipticity, ε_K^s (panel (a)), and the corresponding saturation field, H_s (panel (b)), are plotted versus t_{Fe}. In both plots

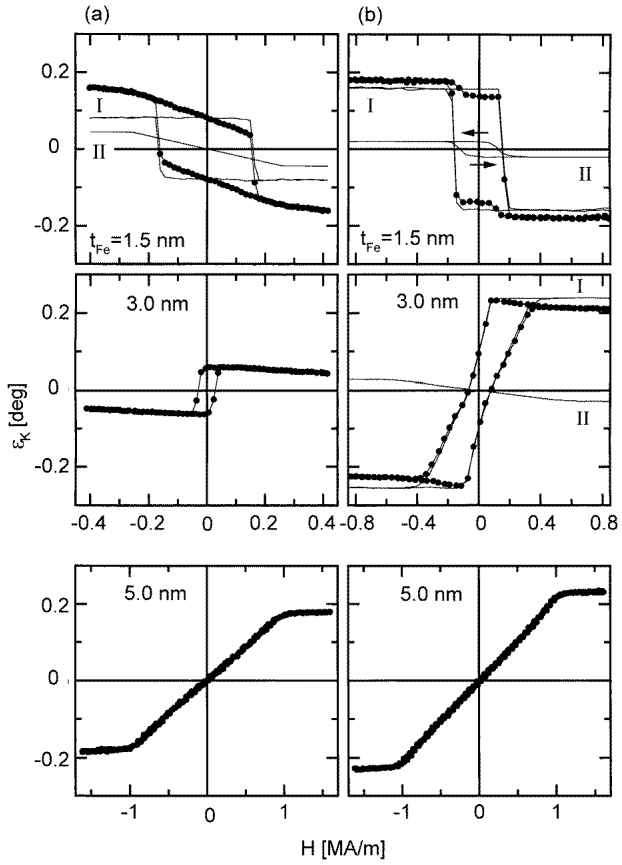

Figure 1. Polar Kerr ellipticity (ε_K) hysteresis loops of the Fe/Tb multilayers evaporated at different substrate temperatures, $T_s = 150$ (panel (a), LT) and 300 K (panel (b), HT) with Tb thickness $t_{Tb} = 1.9$ nm and Fe thicknesses $t_{Fe} = 1.5$, 3.0 and 5.0 nm, obtained at room temperature and light wavelength $\lambda = 633$ nm. Individual components are denoted as I and II (see the text).

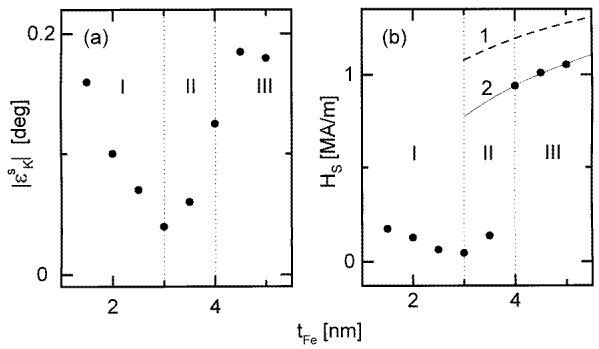

Figure 2. Correlations between magneto-optic and magnetic properties of LT multilayers (figure 1(a)): the saturated polar Kerr ellipticity, ε_K^s (a), and the corresponding saturation magnetic field, H_s (b), versus t_{Fe}. Curves 1 and 2 ((b): broken and solid curves) show model calculations of H_s versus t_{Fe} taking into account the interface thicknesses $t_{a-FeTb} = 0$ and 0.85 nm, respectively.

three regions can be distinguished. For $t_{Fe} \leqslant 3$ nm (region I) fairly low values of both ε_K^s and H_s are encountered. According to conversion-electron Mössbauer spectroscopy (CEMS) measurements [19], the MLs in region I contain a-Fe. On the other hand, for $t_{Fe} \geqslant 4.0$ nm (region III) typical values of $\varepsilon_K^s \approx 0.2^\circ$ and $H_s \approx 1$ MA m^{-1} are observed for crystalline α-Fe [12, 15]. In the changeover range, $3.0 \leqslant t_{Fe} \leqslant 4.0$ nm (region II), a heterogeneous structure of the Fe films might be anticipated. Although crystallization of Fe takes place above the critical thickness, $t_{Fe}^{cr} \approx 3.0$ nm, a certain percentage of Fe remains amorphous [10]. CEMS reveals a fraction of 84% a-Fe in the sample with $t_{Fe} = 3.5$ nm from our LT series [19]. Its relative importance becomes negligible when $t_{Fe} > 4$ nm, i.e. in region III.

Surprisingly, ε_K^s decreases with increasing t_{Fe} in region I (figure 2(a)), although one rather expects a linear increase in the ultrathin-film limit [20]. Obviously this tendency is counteracted by a simultaneous decrease of the saturation magnetization, M_{Fe}^{cr}, at the measurement temperature, RT. This is a consequence of the well-known [21] decrease of the ordering temperature of Fe/Tb MLs with increasing t_{Fe} and involving magnetic interfaces (consisting of amorphous FeTb alloys) and non-magnetic a-Fe (at RT!) in their central regions.

In parallel with the decrease of ε_K^s the saturation field H_s decreases significantly with increasing t_{Fe} in region I (figure 2(b)). It shows a proportionality between H_s and the magnetization of the Fe layers. In the crossover region II, the saturation field steeply rises up to $H_s \approx 1.05$ MA m^{-1} in region III at $t_{Fe} = 5$ nm (figure 2(b)). This value is to be compared with that obtained for bulk thin films of α-Fe, which exhibit $H_s = M_{\alpha-Fe}^s = 1.76$ MA m^{-1} owing to the dominating shape anisotropy and the demagnetization factor $N_\perp = 1$. Two effects are responsible for the reduction of H_s by 38% in the Fe/Tb MLs. First, the total volume, $V = V_{Fe} + V_{Tb}$, which determines the magnetization, is enhanced by the volume of non-magnetic Tb and thus decreases the ratio $M = m/V < M_{\alpha-Fe}^s$. Hence the magnetization of the Tb/Fe MLs is decreased, as represented in figure 2(b) by a broken curve labelled 1. Second, by assuming alloyed interfaces with virtually vanishing moments, the observed variation of H_s versus t_{Fe} can be nearly perfectly modelled with $t_{a-FeTb} = 0.85$ nm (figure 2(b), curve 2) in agreement with previous investigations [9, 12, 15, 22].

The complicated structure of the ε_K^s–H curves obtained for the HT MLs with $t_{Fe} = 1.5$ nm and 3.0 nm (figure 1(b)) can be decomposed into individual components as shown by solid curves denoted as I and II. Let us first discuss the leading contributions, I. They form rectangular and parallelogram-shaped loops for $t_{Fe} = 1.5$ and 3.0 nm, respectively. According to CEMS measurements [19], in both cases strong PMA is indicated by the spin texture angles $\langle\theta\rangle \approx 11^\circ$ with respect to the ML normal. Obviously, a coherent-rotation model seems applicable to the amorphous $t_{Fe} = 1.5$ nm sample [10], whereas for the crystalline $t_{Fe} = 3.0$ nm sample the magnetization reversal probably occurs via domain formation. This is explained by the larger magnetization and, consequently, demagnetization energy, $\mu_0(M_{\alpha-Fe}^s)^2/2$, and explains the fairly low remanence, ε_K^r $(H = 0) \approx 0.4\varepsilon_K^s$.

The second components, II, show small negative saturation Kerr ellipticity, $\varepsilon_K^s \approx -0.02^\circ$, and low saturation fields, $H_s \approx 0.4$ MA m^{-1}, for both cases, $t_{Fe} = 1.5$ nm and 3.0 nm. As discussed previously [12], the novel component obviously reveals soft-magnetic behaviour with weak hysteresis. Its magnetization is only weakly coupled to that of the bulk Fe layers. This is quite obvious for the $t_{Fe} = 1.5$ nm sample, where the Kerr signal II exhibits an unusual switching behaviour when approaching the low-field range (the 'inverse' Kerr loop as indicated by arrows). At $|H| < 0.2$ MA m^{-1} the alignment with the external field (i.e. with the dominant Tb moment) changes into an alignment with the non-dominant a-Fe moments. This crossover from field to exchange coupling is also observed at lower temperatures (figures 3(a) and 3(b)), where it causes the observed asymmetry of the loops II in the vicinity of $|H| \approx 0$ (see section 3.2.1).

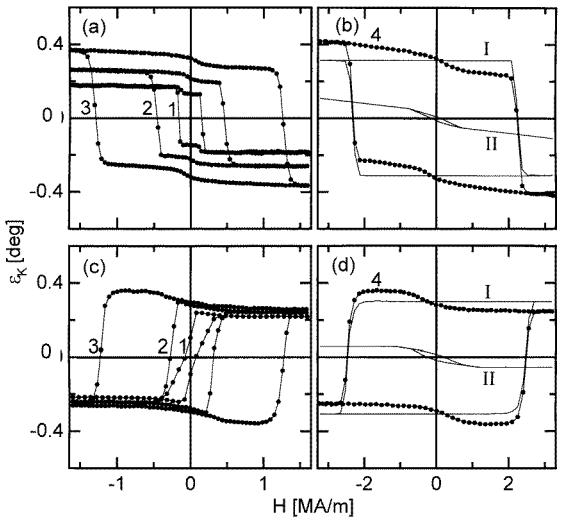

Figure 3. Polar Kerr hysteresis loops of HT multilayers with $t_{Fe} = 1.5$ (panels (a), (b)) and 3.0 nm (panels (c), (d)) measured at different temperatures, 300 (1), 200 (2) 100 (3) and 50 K (4). Curves 4 are decomposed into individual components I and II (solid curves; see the text).

3.2. Temperature dependences

3.2.1. HT multilayers ($T_s = 300$ K). Figure 3 shows the variation with decreasing temperature of the hysteresis loops referring to the HT MLs with $t_{Fe} = 1.5$ (panels (a), (b)) and 3.0 nm (panels (c), (d)). The curves labelled 1 ($T = 300$ K) correspond to those displayed in figure 1(b). Most remarkable is the tremendous increase of their width ($=2H_s$) by a factor of 20 that occurs when cooling from 300 (1) to 50 K (4). Furthermore, the switching behaviour at $\pm H_s$ of the loops becomes more nearly perfect upon cooling in both cases. Both features are consequences of increasing PMA due the increasing polarization of Tb with decreasing T (the Curie temperature of pure Tb is $T_c = 219$ K [23]). In parallel, the amplitudes ε_K^s are strongly increasing between 300 and 50 K. As will be discussed in more detail below, this behaviour is related to the temperature dependence of the saturation magnetization, $M_s \propto \varepsilon_K^s$.

It is interesting to follow the T-dependences of the individual contributions to the Kerr loops discussed above. The decomposition shown in figure 1(b) for $T =$ RT (curves I and II) are encountered in a similar fashion at 50 K (figures 3(b) and 3(d), curves I and II). Despite the different Fe modifications involved, a-Fe and α-Fe for $t_{Fe} = 1.5$ (figure 3(b)) and 3.0 nm (figure 3(d)), the most prominent contributions I reveal very similar characteristics, $H_s \approx 2.2$ MA m^{-1} and $|\varepsilon_K^s| \approx 0.3^\circ$. This clearly hints at the dominating role of the Fe/Tb interfaces. They bear a high potential for PMA in both cases which is transferred by exchange coupling to the bulk of the magnetic Fe layers irrespective of their individual structure, a- or α-Fe.

Interestingly, the 'uncoupled' a-Fe contribution II also survives in both MLs. It remains magnetically soft with an M_r/M_s ratio of about 0.5 and $H_c \approx 0.2$ MA m^{-1}. A closer look reveals that the two contributions, I and II, vary differently with temperature T. This is evident from the plots of ε_K^s versus T in figure 4, where ε_K^s(I) and ε_K^s(II) versus T are obtained by decomposition according to the scheme shown in figures 3(b) and 3(d). It is seen that the weakly coupled a-Fe contributions II (open circles) vary but slightly when cooling from 300 to 50 K. Both exhibit the same sign (note that $|\varepsilon_K| = -\varepsilon_K$ is plotted in figure 4(a)!) and

saturate smoothly at low T, $\varepsilon_K^s(\mathrm{II}, T = 50\ \mathrm{K}) \approx -0.05^\circ$. These observations are consistent with magnetic saturation of a novel modification of a-Fe with $T_c >$ RT in agreement with observations on Fe/Tb MLs containing Ag blocking layers [12]. As discussed above, the observed asymmetry of the type-II magnetization loops is caused by their crossover from field to exchange coupling.

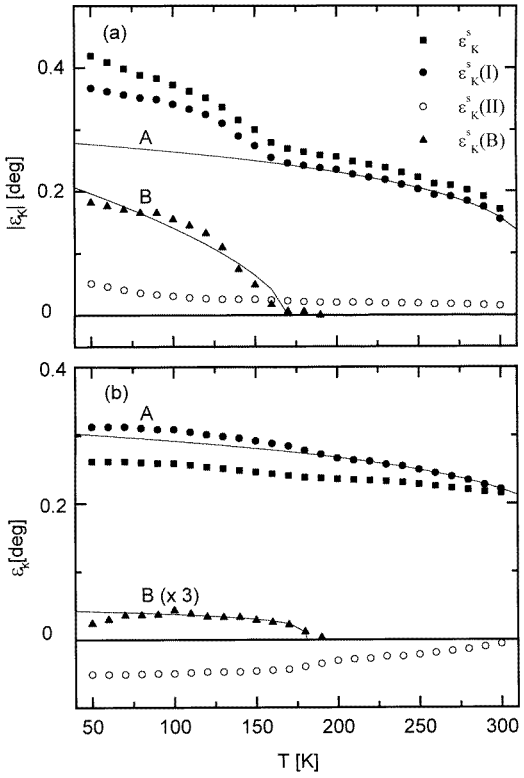

Figure 4. ε_K^s versus T for HT MLs with $t_{Fe} = 1.5$ (a) and 3.0 nm (b) measured within the range $50 \leqslant T \leqslant 300$ K (solid squares). After subtracting $\varepsilon_K^s(\mathrm{II})$ versus T for weakly coupled a-Fe (open circles), the $\varepsilon_K^s(\mathrm{I})$ versus T data (solid circles) are decomposed into the power-law functions (solid curves) labelled A (best fitted within $210 \leqslant T \leqslant 300$ K) and B (best fitted within $70 \leqslant T \leqslant 150$ K).

The contributions $\varepsilon_K^s(\mathrm{I})$ versus T (full circles) reveal two superimposed convex-shaped contributions of the form $\varepsilon_K^s(T) = \varepsilon_K^s(0)(1 - T/T_c)^\beta$ with vertices at high ($T_c^{(A)} \approx 330$ K) and intermediate temperatures ($T_c^{(B)} \approx 180$ K). The low-T contribution appears much more pronounced in the case where $t_{Fe} = 1.5$ nm. Best fits of the data within $210 \leqslant T \leqslant 300$ K (figures 4(a) and 4(b), solid curves) are first used to extract the characteristics of the high-temperature phase A. We find $T_c^{(A)} = 322 \pm 9$ K for $t_{Fe} = 1.5$ nm. The 'critical' exponent is surprisingly small, $\beta^{(A)} = 0.22 \pm 0.04$. Similarly, we find $T_c^{(A)} = 346 \pm 9$ K and $\beta^{(A)} = 0.17 \pm 0.02$ from the data referring to $t_{Fe} = 3.0$ nm and $210 \leqslant T \leqslant 300$ K.

It is tempting to interpret the exponents β in terms of the two-dimensional Ising model (2dIM), for which $\beta = 1/8$ [24]. In fact, the ultrathin Fe/Tb interfaces are no more than two atomic layers thick [22] and show very strong PMA. The following arguments support our conjecture:

(a) The extrapolated values of $T_c \approx 330$ K lie close to that for $Fe_{0.5}Tb_{0.5}$ [25]. This seems to imply that the interface is either atomically smooth with Fe–Tb pairs dominating the exchange interaction, or corrugated to a depth of no more than two atomic layers. Both kinds of interface are found in MBE-grown crystalline Fe/Tb MLs, namely rough Fe-on-Tb and smooth Tb-on-Fe layers [26], whereas only rough interfaces occur in amorphous HT MLs [11]. Moreover, a linear relationship between ε_K^s and the average hyperfine field [4] allows us to predict its value, $B_{hf} = 16.3$ T, from the measured value of $\varepsilon_K^s(300\ K)$. It is close to $B_{hf}(Fe_{0.5}Tb_{0.5}) = 15.5$ T, measured by CEMS [27] and calculated within a molecular-field approach [28].

(b) Although the power law should fail at some distance from T_c, it is favoured by numerous examples in magnetic thin-film physics with meaningful critical exponents β [29]. At least their order of magnitude is indicative of the universality class involved. Obviously the 3d Ising and Heisenberg models, with $\beta = 0.325$ and 0.365, respectively [30], are definitely ruled out.

(c) After subtracting the high-T contributions, $\varepsilon_K^s(A)$, from $\varepsilon_K^s(I)$ versus T we obtain the low-T contributions, $\varepsilon_K^s(B)$, which may, again, be fitted to the above power law. We find $T_c^{(B)} = 170 \pm 2$ K and 180 ± 1 K, $\beta^{(B)} = 0.62 \pm 0.08$ and 0.23 ± 0.05, for $t_{Fe} = 1.5$ and 3.0 nm, respectively. Obviously a second component showing more or less 3d ferromagnetic behaviour undergoes a low-T phase transition. According to our above discussion it appears plausible to attribute these contributions to a-Fe ($T_c \approx 200$ K) [31], which dominates the bulk of the Fe layers when $t_{Fe} = 1.5$ nm, but constitutes only a small fraction when $t_{Fe} = 3.0$ nm. This result agrees with inferences from recent Mössbauer studies [11].

3.2.2. LT multilayers ($T_s = 150$ K) One major effect of the condensation temperature T_s on the properties of Fe/Tb MLs is the difference in the critical thickness, t_{Fe}^{cr}, above which crystallization of α-Fe takes place. Whereas $t_{Fe} = 3$ nm yields crystalline layers if $T_s = 300$ K, they are still amorphous at $T_s = 150$ K. As discussed in section 3.1, this situation gives rise to a rectangular hysteresis cycle (figure 1(a)) owing to strong surface-induced PMA due to exchange-coupled Fe/Tb pairs [32].

Upon cooling to below RT, the Kerr optical hysteresis loops exhibit very complex changes. As is shown for the LT ML with $t_{Fe} = 3$ nm in figure 5 for temperatures ranging between 250 and 160 K, the most drastic changes occur between 210 and 180 K. As will be discussed below in more detail, the observed anomalies of the ε_K–H curves result from two peculiarities of the a-Fe/Tb system:

(a) Tb becomes ferromagnetic below $T_c = 219$ K [23], where it starts to dominate the magnetization of the Fe/Tb interfaces via ferrimagnetic exchange coupling;

(b) a-Fe becomes ferromagnetic below $T_c \approx 200$ K [31], couples to the Fe/Tb interfaces and increasingly contributes to the total Kerr ellipticity.

A first signature of magnetic heterogeneity of our LT ML (figure 5) is observed at $T = 250$ K, where the Kerr loop sharply bends up just before reaching the switching field, $H_s \approx -0.5$ MA m^{-1}. The same feature, namely a linear decrease of ε_K versus H in the vicinity of $H = 0$, is observed with similar intensity for all Kerr loops depicted in figure 5. We attribute this anomaly to a virtually uncoupled a-Fe component in analogy to that of the component II found in the case of the HT MLs (figures 3(b) and 3(d)). This contribution reveals, again, negative Kerr ellipticity with nearly constant amplitude, $\varepsilon_K \approx -0.15^\circ$, and a switching field $H_s \approx 0.5$ MA m^{-1} below its ordering temperature, $250 < T_c < 300$ K (the dashed curves denoted as II in figure 5, for $T < 210$ K).

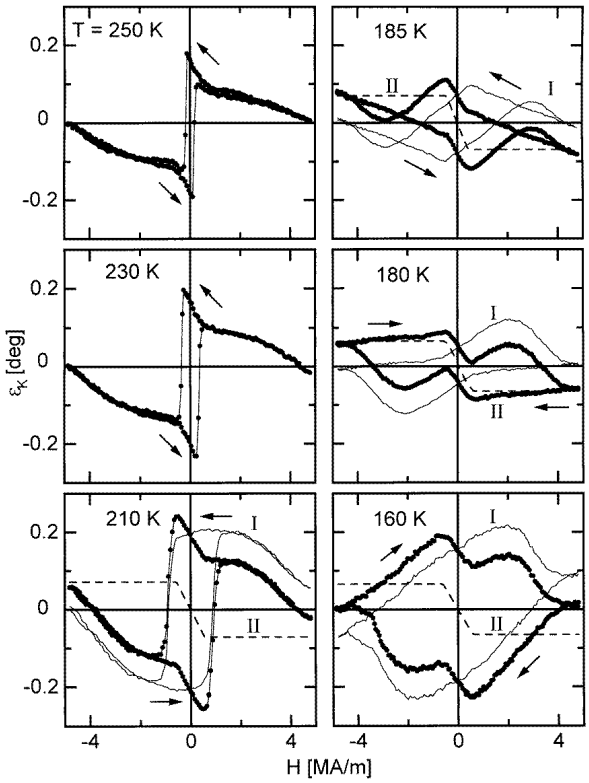

Figure 5. Polar Kerr hysteresis loops of a LT multilayer with $t_{Fe} = 3.0$ nm measured in the directions of the arrows at different temperatures, $160 \leqslant T \leqslant 250$ K. The curves I (thin solid curves for $210 \geqslant T \geqslant 160$ K) refer to the measured ones (solid circles) after subtracting contributions due to weakly coupled a-Fe (curves II, broken curves; see the text).

The difference curves labelled as I in figure 5 exhibit three important features:

(a) the coercive field increases from $H_c \approx 1$ to 3 MA m^{-1} when cooling from 210 to 160 K;
(b) the remanence, ε_K^r, changes sign upon cooling, and achieves its lowest values at $T \approx 180$ K;
(c) as a rule (except at $T \approx 180$ K), the saturation values ε_K^s at $H = 5$ MA m^{-1} are lower than ε_K^r.

Assuming that the Kerr ellipticity signals are exclusively due to Fe, while the contributions due to Tb are neglected [16], we argue first for the limiting cases at 210 and 160 K.

At $T = 210$ K the large positive Kerr remanence, $\varepsilon_K^r = 0.2^\circ$, proves dominance of the Fe moments in the ferrimagnetically coupled interfaces. A plot of ε_K^r versus T (not shown) can be extrapolated to higher temperatures using a power law with a Curie temperature $T_c = 301$ K and a critical exponent $\beta = 0.39 \pm 0.03$. These data are consistent with Tb-rich amorphous $Fe_{0.4}Tb_{0.6}$ [25] forming an extended interface with 3d magnetic behaviour. This contrasts with the 2d magnetism observed at the much sharper HT ML interfaces (section 3.2.1), the smoothness of which results from phase segregation by thermally activated diffusion.

Surprisingly, the Kerr signal starts to decrease at $H > 2$ MA m^{-1} and nearly vanishes as $H \to 5$ MA m^{-1}. Very probably, because the temperature is close to the ordering temperature of Tb, $T_c = 219$ K [23], the highly susceptible Tb component becomes increasingly polarized

and eventually gains Zeeman energy when being turned towards the direction of $\boldsymbol{H}$. The inverted ferrimagnetically coupled Fe component now gradually contributes with a negative sign to ε_K.

On lowering the temperature to $T = 160$ K, both Tb and a-Fe are spontaneously ordered and thus provide full exchange coupling between the Fe/Tb interfaces. As a consequence, the coercive force increases drastically, $H_c \approx 4$ MA m^{-1}. Owing to the Tb dominance, a negative remanence signal, $\varepsilon_K^r = -0.2^\circ$, is encountered. Peculiarly, however, the Kerr loop, curve I, is inclined with respect to the H-axis by about 45° such that the saturated value at $H = 5$ MA m^{-1} becomes weakly positive. Obviously the Kerr signal becomes overcompensated by virtue of the two Fe contributions with different polar orientations. Since the exchange coupling between Fe and Tb ($T_c > 300$ K) is much stronger than that between the interface parts and the bulk of the Fe layers ($T_c \approx 200$ K), the latter one is probably easily broken by the external field. Hence, with increasing field H the moments of the inner part of the Fe layers turn towards the direction of $\boldsymbol{H}$, whereas the Fe moments adjacent to the Tb layers stay antiparallel to both $\boldsymbol{H}$ and the Tb moments. This mechanism explains the near inversion of the Kerr ellipticity at maximum field. Much higher fields are required to break the exchange coupling within the Fe/Tb interface alloys and to achieve positive saturation.

At intermediate temperatures, $180 \leqslant T \leqslant 185$ K, the Kerr loops, curves I, reflect crossover situations. Remarkably, the Kerr remanence, ε_K^r, does not switch abruptly from $+0.2^\circ$ to -0.2°, as expected in the situation of a global compensation temperature [13]. Instead, a gradual decrease of ε_K^r occurs within a temperature interval of about 40 K and becomes gradually inverted towards negative values at $T < T_c(\text{Tb}) \approx 219$ K.

The decrease of ε_K^r suggests that the global Kerr signal is cancelled by the superposition of positive and negative contributions relating to the limiting cases discussed above. Since the Fe/Tb interfaces are intermixed with various effective concentrations, it seems plausible to assume a polydomain-like picture of the ML system, partially strongly coupled and Tb dominated as observed at 160 K, partially still in the essentially uncoupled, Fe-dominated interface regime as observed at 210 K. This view is corroborated by a tentative linear superposition of the limiting cases, $\varepsilon_K(210\text{ K}) \equiv \varepsilon_h$ and $\varepsilon_K(160\text{ K}) \equiv \varepsilon_l$, performed in order to simulate ε_K versus H at intermediate temperatures. Figure 6 shows the model functions $\varepsilon_K(185\text{ K}) = 0.45\varepsilon_h + 0.1\varepsilon_l$ and $\varepsilon_K(180\text{ K}) = 0.12\varepsilon_h + 0.4\varepsilon_l$ (solid curves) together with the corresponding experimental curves I (solid circles; figure 5). Obviously, many features of the experimental data are satisfactorily reproduced. The absence of sharp jumps occurring in ε_K versus H at $T \geqslant 210$ K (figure 5) is probably due to multidomain processes, which give rise to sheared hysteresis loops as observed throughout the crossover range (e.g. at $T = 195$ K; see the inset in figure 6(a)).

4. Conclusions

It has been shown that the growth conditions of Fe/Tb MLs play an important role not only as regards the structure of the Fe layers, but also as regards the morphology and the magnetic properties of the alloyed interfaces. Obviously, they are much thinner in HT MLs than in the case of LT-grown MLs. This difference seems crucial to their effective dimensionality in the temperature range $T_c(\text{a-Fe}) \approx 200\text{ K} < T < T_c(\text{Fe/Tb}) \approx 330$ K, where they can be considered as isolated magnetic subsystems. Typical 2d Ising model exponents of the magnetization, $\beta \approx 0.2$, emerge for the HT-type interfaces, whereas 3d behaviour is reflected by values of $\beta > 0.3$ for the LT-type case. Owing to the thick interfaces encountered in LT MLs, crystallization of Fe requires substantially larger single-layer thickness, t_{Fe}, than in HT MLs.

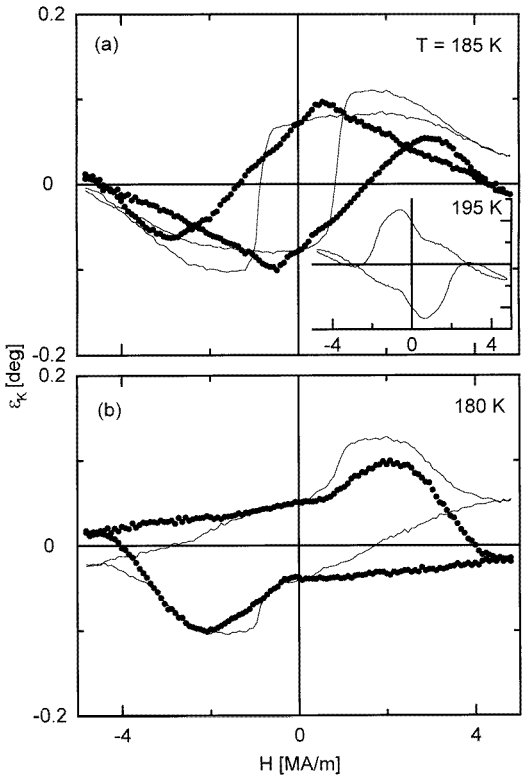

Figure 6. Curves I referring to the polar Kerr hysteresis loops of a LT multilayer with $t_{Fe} = 3.0$ nm obtained for $T = 185$ K (a) and 180 K (b) (solid circles; see figure 5) and modelled by linear combinations of the curves I obtained at $T = 160$ and 210 K (see the text). Inset: the uncorrected polar Kerr hysteresis loop of a LT multilayer with $t_{Fe} = 3.0$ nm measured at $T = 195$ K.

Peculiarities of the hysteresis cycles are encountered at compensation transitions of the ferrimagnetically coupled Fe/Tb system. Such a case has been realized by choosing LT conditions and $t_{Fe} = 3$ nm. Here the high-T dominance of Fe is replaced by Tb dominance below 200 K. In a broad crossover regime between 210 and 160 K, the simultaneous growth of ferromagnetic long-range order for both Tb ($T_c = 219$ K) and a-Fe ($T_c \approx 200$ K) gives rise to smearing of the compensation transition. This is, e.g., evident from the gradual change of the remnant Kerr ellipticity between $+0.2^\circ$ and -0.2°.

In addition, two novel field-induced phenomena are reported:

(a) At $T > 210$ K the Fe dominance of the magnetic moments is broken in the absence of exchange coupling between the interfaces by field-induced polarization of highly susceptible Tb. Inversion of the magnetization curve, ε_K versus H, is observed in high fields.

(b) In the presence of exchange coupling between the interfaces via the spontaneously magnetized layers of both Tb and a-Fe at $T \approx 160$ K, the antiparallel arrangement between the Fe moments and the dominating Tb moments is partially broken by an external magnetic field. At $H \approx 4$ MA m^{-1} one observes decoupling of the bulk a-Fe moments from those in the interface. As a consequence the total magneto-optical response is nearly cancelled. Higher fields, $H > 5$ MA m^{-1}, are required to also break the exchange coupling

between Tb and Fe within the interfaces until all moments are aligned and maximum ε_K is achieved.

(c) Throughout this investigation we have used the fact that the Kerr ellipticity at the photon energy used, $E \approx 2$ eV, is primarily sensitive to the magnetic moment of Fe contained in the MLs. This has the advantage of making it easier to follow the individual magnetic behaviours of the Fe component. However, in order to understand the complete process of magnetization reversal in Fe/Tb MLs, it will be necessary to also study that of the Tb component, either by measuring the global magnetization, e.g. by SQUID magnetometry, or by investigating the Kerr signal at higher photon energies [33].

Acknowledgments

The authors are indebted to U von Hörsten and F Richomme for preparation of the samples and discussions, and to M Aderholz for technical assistance. This work was supported by the Deutsche Forschungsgemeinschaft through SFB 166.

References

[1] Tanaka M, Yuzurihara H and Tokita T 1987 *IEEE Trans. Magn.* **23** 2955
[2] Shi L, Ji Z R and Hu L 1991 *J. Appl. Phys.* **69** 5313
[3] Mibu K, Hosoito N and Shinjo T 1993 *J. Magn. Magn. Mater.* **126** 343
[4] Fnidiki A, Richomme F, Teillet J, Pierre F, Boher P and Houdy Ph 1993 *J. Magn. Magn. Mater.* **121** 520
[5] Scholz B, Brand R A and Keune W 1991 *Hyperfine Interact.* **68** 409
[6] Kim W S, Kleemann W, von Hörsten U and Keune W 1995 *Proc. 3rd Int. Symp. on Physics of Magnetic Materials (Seoul)* ed C S Kim, T D Lee and J H Oh (Seoul: Korean Magn. Soc.) p 982
[7] Marks O, Voiron J, Ruckert T, Tappert J, Keune W, Kim W S and Kleemann W 1998 *IEEE Trans. Magn.* **34** 834
[8] Malmhäll R and Chen T 1982 *J. Appl. Phys.* **53** 7843 and references therein
[9] Cherifi K, Dufour C, Piecuch M, Bruson A, Bauer Ph, Marchal G and Mangin Ph 1991 *J. Magn. Magn. Mater.* **93** 609
[10] Dufour C, Cherifi K, Bruson A, Marchal G and Mangin Ph 1991 *Phys. Status Solidi* a **125** 561
[11] Richomme F, Scholz B, Brand R A, Keune W and Teillet J 1996 *J. Magn. Magn. Mater.* **156** 195
[12] Kim W S, Kleemann W, Tappert J and Keune W 1998 *J. Appl. Phys.* **84** 4384
[13] Reim W and Weller D 1988 *IEEE Trans. Magn.* **24** 2308
[14] Kim W S, Aderholz M and Kleemann W 1993 *Meas. Sci. Technol.* **4** 1275
[15] Kim W S, Andrä W and Kleemann W 1998 *Phys. Rev.* B **58** 6346
[16] Challener W A 1990 *J. Appl. Phys.* **67** 4441
[17] Carbone C, Rochow R, Braicovich L, Jungblut R, Kachel T, Tillmann D and Kisker E 1990 *Phys. Rev.* B **41** 3866
[18] Pierre F, Boher P, Kergoat H, Houdy Ph, Ferré J and Pénissard G 1991 *J. Appl. Phys.* **69** 4565
[19] Richomme F 1997 unpublished
[20] Višnovský Š, Nývlt M, Prosser V, Lopušník R, Urban R, Ferré J, Pénissard G, Renard D and Krishnan R 1995 *Phys. Rev.* B **52** 1090
[21] Honda S, Kimura T and Nawate M 1993 *J. Magn. Magn. Mater.* **121** 116
[22] Scholz B, Brand R A and Keune W 1994 *Phys. Rev.* B **50** 2537
[23] Elliot R J 1972 *Magnetic Properties of Rare Earth Metals* (London: Plenum)
[24] Onsager L 1944 *Phys. Rev.* **65** 117
Yang C N 1952 *Phys. Rev.* **85** 808
[25] Hansen P, Clausen C, Much G, Rosenkranz M and Witter K 1989 *J. Appl. Phys.* **66** 756
[26] Tappert J, Jungermann J, Scholz B, Brand R A and Keune W 1994 *J. Appl. Phys.* **76** 6293
[27] Ruckert T, Tappert J, Brand R A and Keune W 1997 *J. Magn. Magn. Mater.* **165** 411
[28] Heiman N, Lee K, Potter R I and Kirkpatrick S 1976 *J. Appl. Phys.* **47** 2634
[29] Kohlhepp J, Elmers H J, Cordes S and Gradmann U 1992 *Phys. Rev.* B **45** 12 287
Li Y and Baberschke K 1992 *Phys. Rev. Lett.* **68** 1208
Rau C, Mahavadi P and Lu M Z 1993 *J. Appl. Phys.* **73** 6757
[30] Ma S K 1976 *Modern Theory of Critical Phenomena* (New York: Benjamin)

[31] Alperin H A, Cullen J R and Clark A E 1976 *AIP Conf. Proc*. **29** 186
Richomme F, Teillet J, Fnidiki A, Auric P and Houdy Ph 1996 *Phys. Rev.* B **54** 416
[32] Sato N 1986 *J. Appl. Phys.* **59** 2514
[33] Katayama T and Hasegawa K 1982 *Rapidly Quenched Metals IV* ed T Matsumoto and K Suzuki (Sendai: Japanese Institute of Metals) p 915